Systematic study of anisotropic magnetoresistance in (Ga,Mn)As

Zdeněk Kašpar[1,2], Kamil Olejník[2], Karel Výborný[2], Helena Reichlová[2], Miroslav Maryško[2], and Vít Novák[2]

[1] Faculty of Mathematics and Physics, Charles University in Prague, Ke Karlovu 3, CZ–12116 Praha 2, Czech Republic
[2] Institute of Physics ASCR, Cukrovarnická 10, CZ–16253 Praha 6, Czech Republic

Abstract

We systematically study the anisotropic magnetoresistance (AMR) on a series of optimized (Ga,Mn)As samples. The crystalline and non-crystalline contributions to the AMR were separated and an apparent higher-order term (of six-fold symmetry) was identified to be an artefact resulting from the presence of magnetic anisotropy of the material and of the residual fields of external superconducting magnets. In the broad range of nominal Mn concentrations from 2% to 11%, we find the non-crystalline contribution to dominate, although the crystalline terms become relatively more important for higher doping levels. We compare the AMR magnitude with the Boltzmann transport calculations based on the $k \cdot p$ mean-field kinetic-exchange model.

Keywords: anisotropic magnetoresistance, magnetic anisotropy, diluted magnetic semiconductor, (Ga,Mn)As, transport measurement

1 Introduction

Although low Curie temperature limits the practical use of (Ga,Mn)As, this material proved as a good test bed for exploring spintronic device concepts [5]. It is a dilute magnetic semiconductor based on the well explored GaAs host with which it shares many similar properties [3] such as the crystal structure or direct band gap. The Mn atoms substituting gallium in the lattice, however, create a relatively strong disorder so that (Ga,Mn)As behaves in some aspects like a dirty metal rather than a semiconductor. Nevertheless, (Ga,Mn)As inherits from its host a strong spin-orbit interaction so, similar to ferromagnetic metals [8], anisotropic magnetoresistance (AMR) is observed also in (Ga,Mn)As.

By measuring the AMR, we can read the direction of magnetisation. Apart from practical applications of this concept such as detectors for parked cars, spin-orbit driven ferromagnetic resonance [2] or determination of magnetic anisotropy [7, 6] can be mentioned as examples of its utility in basic research. First observation of the anisotropic behaviour of resistivity in (Ga,Mn)As was published in 2002 [1]. Theoretical description of the effect is based on the
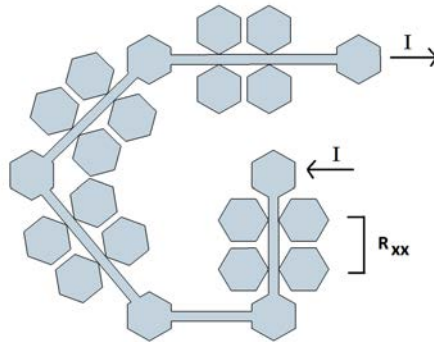
Figure 1: Mask used for optical lithography. Hallbar width is 100 μm, length 500 μm.

Wafer	Mn doping [%]	d [nm]	T_c [K]	$\mu_0 H_c$ [mT]	$\mu_0 H_u$ [mT]	σ_0 [$(\Omega\text{cm})^{-1}$]
J052	2	20	63.7			254
J040	3	20	93.5	80.5	45.0	435
J039	5	20	147.0	24.2	18.4	557
J018	7.1	20	175.0	8.5	18.4	530
J030	9	20	186.2	4.5	23.7	483
J033	10.9	16	186.7	6.8	18.2	370

Table 1: Sample parameters described in the text.

Boltzmann equation formalism [4] and it allowed to identify the highly anisotropic scattering rates as the main source of the dominant non-crystalline part of the AMR in (Ga,Mn)As [13]. It depends on various parameters that can be controlled during sample preparation and this work is an update in the exploration of this dependence.

2   Samples and Measurement method

This work investigates a series of (Ga,Mn)As samples with nominal Mn concentration x ranging from 2% to 11%. The samples were grown by molecular beam epitaxy on a GaAs substrate. In order to achieve the highest possible Curie temperature, samples were annealed [9]. By optical lithography, 100 μm wide Hall bars were fabricated oriented along different crystallographic orientations (G-shaped mask is shown in Fig. 1). For a better conducting standard layer (5 nm Cr and 35 nm Au) was deposited on the top of the contact pads.

In table 1, some parameters of the used samples are given: thickness d of the (Ga,Mn)As layer, Curie temperature T_C, magnetic anisotropy cubic (H_c) and uniaxial components H_u and the averaged conductance σ_0. Anisotropy constants and T_c were obtained from SQUID measurement, the former are defined according to

$$E(\psi) = \mu_0 H_u M_s \sin 2\psi + \frac{1}{4}\mu_0 H_c M_s \cos 4\psi - \mu_0 H_{ext} M_s \cos(\psi - \psi_{ext}) \tag{1}$$

where M_s is the saturation magnetisation, μ_0 the vacuum permeability and ψ (ψ_{ext}) is the magnetisation (magnetic field) angle, measured from the [100] crystallographic direction.

Term/Hall bar direction	110	1$\bar{1}$0	100	010
K_{c2}	$C_I + C_{IC}$	$C_I + C_{IC}$	$C_I - C_{IC}$	$C_I - C_{IC}$
K_{c4}	C_C	C_C	$-C_C$	$-C_C$

Table 2: AMR component identification: relationship between constants in Eq. (2) and Eq. (3).
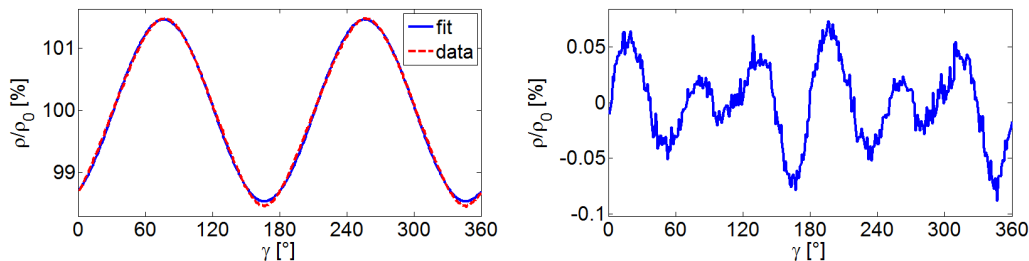
Figure 2: Measured angular dependence of resistivity in the $x = 3$ % sample and identification of the component with sixfold symmetry.

The superconducting vector magnet, equipped with three perpendicular independent magnets, was used to manipulate the sample magnetisation. The field was always oriented in-plane, its magnitude was 1 T and we measured the longitudinal voltage using four terminal method at a constant current of $50\mu A$. An example of the measured resistance variation is shown in the left panel of Fig. 2. The dependence on doping was measured at 10 K and the temperature dependence was taken in the range from 5 K to 75 K.

3 Results

Longitudinal resistance was measured as a function of the angle γ between the applied field $\vec{B}$ and current and the measured data $\rho(\gamma)$ was fitted by the least square method using formula inferred from Ref. [11]. Since the residual part showed a clear signal with six-fold symmetry (see the right panel in Fig. 2), we used

$$\frac{\rho}{\rho_0} = 1 + K_{c2}\cos 2\gamma + K_{c4}\cos 4\gamma + K_{s4}\sin 4\gamma + K_6\cos 6\gamma \tag{2}$$

for fitting where $\rho_0 = 1/\sigma_0$ is the resistance averaged over the in-plane rotation of $\vec{B}$.

The equation for AMR as a function of the angle ψ between magnetisation direction and $\hat{x}$ (crystallographic direction [100]) has the form [10]

$$\frac{\rho}{\rho_0} = 1 + C_I\cos(2\psi - 2\theta) + C_{IC}\cos(2\psi + 2\theta) + C_C\cos 4\psi \tag{3}$$

where θ identifies the Hall bar direction (as an angle between current and $\hat{x}$). We can associate the non-crystalline C_I, cubic-crystalline C_C and first order crossed term C_{IC} to terms K_{c2} and K_{c4} as it follows from Tab. 2. Origin of the last term in Eq. (2) will be discussed later.

Values of AMR constants C_I, C_{IC} and C_C obtained by this procedure are plotted on the left panel in Fig. 3 as a function of the nominal sample doping x. The non-crystalline term (C_I) is dominant although C_{IC} becomes appreciable at lower x. The cubic crystalline AMR term
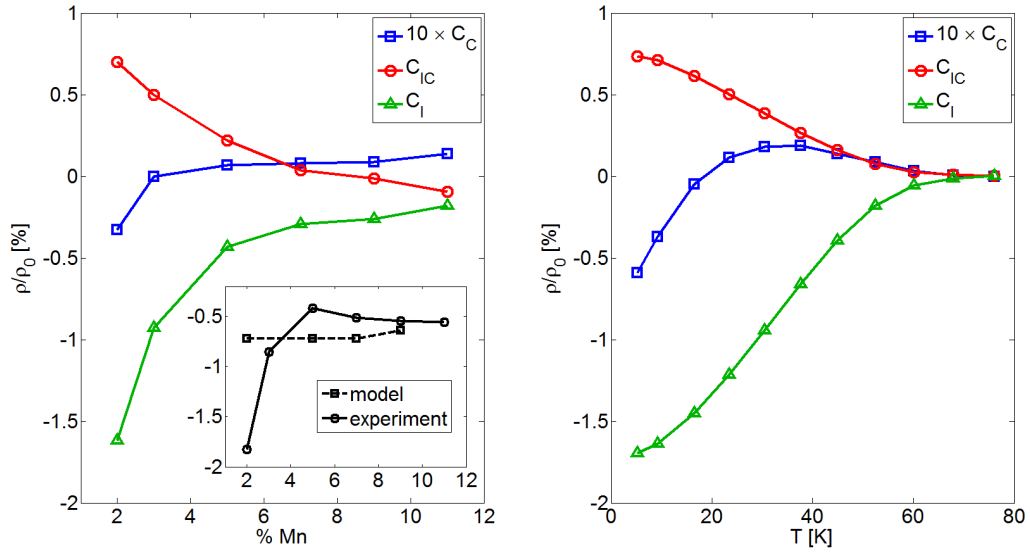
Figure 3: Doping and temperature dependence of the AMR components defined in Eq. (3). The left panel refers to measurements at $T = 10$ K, the inset shows theoretically calculated $2(\rho_\parallel - \rho_\perp)/(\rho_\parallel + \rho_\perp)$ (assuming the validity of Matthiessen's rule) compared to the corresponding experimental values. The right panel shows data for the $x = 2\%$ sample.

C_C is an order of magnitude smaller and shows a non-monotonic temperature dependence (see right panel of Fig. 3). In total, the longitudinal AMR is close to the popular $\rho/\rho_0 - 1 \propto \cos^2 \phi$ form [12] for all samples where $\phi = \psi - \theta$ is the angle between magnetisation and current. Crystalline components are small and special care needs to be taken to distinguish them from various artefacts discussed in the following section. All AMR components become small as temperature approaches T_C (right panel of Fig. 3).

Calculations of the AMR based on the Boltzmann equation [13] corrected to the experimentally determined conductivity σ_0 agree well with the data in Fig. 3. Assuming that the carriers scatter only from the substitutional Mn (contrary to other defects, these are likely to cause anisotropic transport since they contribute to M_s), conductivity calculated without any fitting parameters is about an order-of-magnitude larger than the experimental values in Tab. 1 This implies that some scattering mechanisms have been omitted in this description. Rather than attempting to microscopically describe the scattering from other possible defects [4] whose densities are not known in detail, we correct the calculated conductivity assuming the validity of Matthiessen's rule. Because of the large denominator, the values of $2(\rho_\parallel - \rho_\perp)/(\rho_\parallel + \rho_\perp)$ then drop to the level of tenths of per cent and approach the experimental values shown in the inset in Fig. 3. Resistivities in the direction parallel ($\rho_\parallel$) and perpendicular ($\rho_\perp$) to the magnetisation were calculated assuming current direction along $\hat{x}$. Density of substitutional Mn in the calculations (which influences both the ferromagnetic splitting and scattering rates evaluated from the Fermi golden rule) was inferred from M_s as measured by SQUID rather than from nominal doping. Values of Luttinger parameters (which enter the model as described in Ref. [13]) were $\gamma_1 = 6.98$, $\gamma_2 = 2.06$ and $\gamma_3 = 2.93$. Strain effects were neglected.
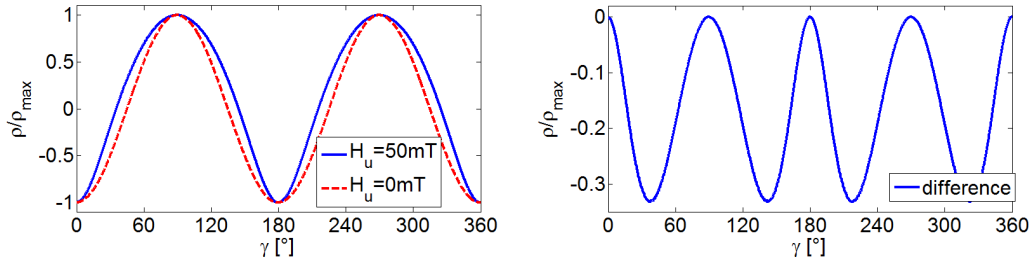
Figure 4: Simulation of the influence of uniaxial magnetic anisotropy as described in the text.

4   Artefacts in signal

When fitting the data, we detected a six-fold symmetry term $\cos 6\psi$ and an unphysical four-fold symmetry term $\sin 4\psi$. The former can in principle be present in cubic materials as Eq. (A.4) in Ref [10] implies. However, we relate these terms to artefacts resulting from the presence of magnetic anisotropy and hysteresis of the superconducting magnets.

If the magnetic anisotropy is not negligible compared to the external magnetic field $|\vec{B}|$, the magnetisation vector is not aligned precisely along $\vec{B}$. This is illustrated in the left panel of Fig. 4 which shows a simulation of this effect in case of purely non-crystalline AMR (only $C_I \neq 0$). The external field magnitude was 300 mT and uniaxial anisotropy 0 mT (red) or 50 mT (blue). As expected, the red curve has $\cos 2(\psi - \theta)$ dependence, while blue curve differs from it. The difference is shown in Fig.4 (right), it contains obvious four-fold symmetry contribution.

Another possible artefact result from the hysteresis of the superconducting magnets. We have simulated hysteresis of both in-plane magnets using non-zero residual field B_{hyst}. The left panel of Fig. 5 shows hysteretic dependence of magnetic field of single superconducting magnet on nominal magnetic field (nominal current). To illustrate the effect we have calculated hysteresis with residual field of 300 mT (the residual field is in reality only about 50 mT). The consequence of this hysteresis is a non-trivial distortion of the rotating magnetic field shown in the right panel of Fig. 5. When AMR is simulated with the distorted field we again observe a deviation from the $\cos(2\psi - 2\theta)$ dependence.

To elucidate the influence of the two effects, we performed a set of simulations of angular dependences of resistance of a bar oriented along the [110] crystallographic direction. For illustration, we assumed in the simulations that the AMR only has the uniaxial non-crystalline term $C_I = 1$. We selectively added and combined the effects of hysteresis of magnets (B_{hyst}) and of uniaxial (H_u) and cubic (H_c) magnetic anisotropies. We fitted the simulated angular dependences with Eq. (2) and summarize the results in Tab. 3.

In the absence of disturbances ($B_{hyst} = B_{uni} = B_{cub} = 0$), the value $K_{c2} = 1$ corresponds to the initial assumption $C_I = 1$. Artefact terms of various symmetries appear due to non-zero B_{hyst}, B_{uni} and B_{cub} as the non-zero entries in Tab. 3) demonstrate. Interestingly, some terms appear only as a combined effect of the hysteresis and magnetic anisotropy.

It is important to note, that the presence of uniaxial anisotropy induces contribution to the K_{C4} term. The contribution has opposite sign for measurements on hall bars along easy [1$\bar{1}$0] and hard [110] directions (in the Tab 3 represented by the change of the anisotropy constant $\mu_0 H_U = 100$ mT to $\mu_0 H_U = -100$ mT). When evaluating the correct value of C_C we averaged the results from bars along [110] and [1$\bar{1}$0] which cancels the contribution of this artefact.
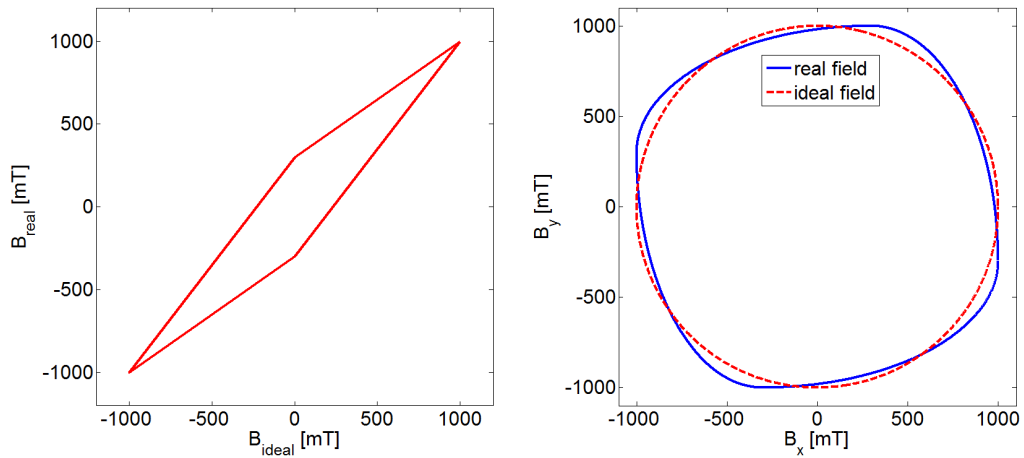
Figure 5: Simulation of the hysteresis of the superconducting magnet used to generate $\vec{B}$.

$B_{hyst}(\mathrm{mT})$	$\mu_0 H_u(\mathrm{mT})$	$\mu_0 H_c(\mathrm{mT})$	K_{c2}	K_{s4}	K_{c4}	K_{s6}	K_{c6}
0	0	0	1	0	0	0	0
50	0	0	0.9985	0	0	0.0105	0.0004
0	100	0	0.8956	0	0.0886	0	0.0131
50	100	0	0.8939	0.0012	0.0883	0.0097	0.0134
0	-100	0	0.8956	0	-0.0886	0	0.0131
50	-100	0	0.8939	-0.0012	-0.0883	0.0097	0.0134
0	0	100	0.9477	0	0	0	0.0456
50	0	100	0.9458	0	0	0.0114	0.0460
0	0	-100	1.0473	0	0	0	-0.0530
50	0	-100	1.0462	0	0	0.0096	-0.0527

Table 3: Simulation of the influence of superconducting magnet hysteresis (B_{hyst}) and magnetic anisotropy on the results of fitting.

5   Conclusion

We have studied AMR on a series of (Ga,Ma)As samples with different nominal Mn doping. We have identified individual components of the AMR and found their dependence on Mn doping and temperature. We have compared measured data with theoretical values calculated using Boltzmann equation and Matthiessen's rule. Terms of unexpected symmetry were found. They are caused by non-negligible magnetic anisotropy and by the hysteresis of the superconducting magnets and they are unrelated to the AMR crystalline components.

References

[1] David V. Baxter, Dmitry Ruzmetov, Julia Scherschligt, Y. Sasaki, X. Liu, J. K. Furdyna, and C. H. Mielke. Anisotropic magnetoresistance in (Ga,Mn)As. *Physical Review B*, 65(21):212407, May 2002.

[2] D. Fang, H. Kurebayashi, J. Wunderlich, K. Výborný, L. P. Zrbo, R. P. Campion, A. Casiraghi, B. L. Gallagher, T. Jungwirth, and A. J. Ferguson. Spin-orbit-driven ferromagnetic resonance. *Nature Nanotechnology*, 6(7):413–417, July 2011.

[3] T. Jungwirth, Jairo Sinova, J. Mašek, J. Kučera, and A. H. MacDonald. Theory of ferromagnetic (III,Mn)V semiconductors. *Reviews of Modern Physics*, 78(3):809–864, August 2006.

[4] T. Jungwirth, Jairo Sinova, K. Y. Wang, K. W. Edmonds, R. P. Campion, B. L. Gallagher, C. T. Foxon, Qian Niu, and A. H. MacDonald. DC-transport properties of ferromagnetic (Ga,Mn)As semiconductors. *Applied Physics Letters*, 83(2):320, 2003. arXiv: cond-mat/0302060.

[5] T. Jungwirth, J. Wunderlich, V. Novák, K. Olejník, B.L. Gallagher, R.P. Campion, K.W. Edmonds, A.W. Rushforth, A.J. Ferguson, and P. Nmec. Spin-dependent phenomena and device concepts explored in (Ga,Mn)As. *Reviews of Modern Physics*, 86(3):855–896, July 2014.

[6] W. Limmer, J. Daeubler, L. Dreher, M. Glunk, W. Schoch, S. Schwaiger, and R. Sauer. Advanced resistivity model for arbitrary magnetization orientation applied to a series of compressive- to tensile-strained (Ga,Mn)As layers. *Physical Review B*, 77(20):205210, May 2008.

[7] W. Limmer, M. Glunk, J. Daeubler, T. Hummel, W. Schoch, R. Sauer, C. Bihler, H. Huebl, M. S. Brandt, and S. T. B. Goennenwein. Angle-dependent magnetotransport in cubic and tetragonal ferromagnets: Application to (001) and (113) oriented Ga,Mn)As. *Physical Review B*, 74(20):205205, November 2006.

[8] T.R. McGuire and R.I. Potter. Anisotropic magnetoresistance in ferromagnetic 3d alloys. *IEEE Transactions on Magnetics*, 11(4):1018–1038, July 1975.

[9] K. Olejník, M. H. S. Owen, V. Novák, J. Mašek, A. C. Irvine, J. Wunderlich, and T. Jungwirth. Enhanced annealing, high Curie temperature, and low-voltage gating in (Ga,Mn)As: A surface oxide control study. *Physical Review B*, 78(5):054403, August 2008.

[10] E. De Ranieri, A. W. Rushforth, K. Výborný, U. Rana, E. Ahmad, R. P. Campion, C. T. Foxon, B. L. Gallagher, A. C. Irvine, J. Wunderlich, and T. Jungwirth. Lithographically and electrically controlled strain effects on anisotropic magnetoresistance in (Ga,Mn)As. *New Journal of Physics*, 10(6):065003, June 2008.

[11] A. W. Rushforth, K. Výborný, C. S. King, K. W. Edmonds, R. P. Campion, C. T. Foxon, J. Wunderlich, A. C. Irvine, P. Vašek, V. Novák, K. Olejník, Jairo Sinova, T. Jungwirth, and B. L. Gallagher. Anisotropic Magnetoresistance Components in (Ga,Mn)As. *Physical Review Letters*, 99(14):147207, October 2007.

[12] H. X. Tang, R. K. Kawakami, D. D. Awschalom, and M. L. Roukes. Giant Planar Hall Effect in Epitaxial (Ga,Mn)As Devices. *Physical Review Letters*, 90(10):107201, March 2003.

[13] Karel Výborný, Jan Kučera, Jairo Sinova, A. W. Rushforth, B. L. Gallagher, and T. Jungwirth. Microscopic mechanism of the noncrystalline anisotropic magnetoresistance in (Ga,Mn)As. *Physical Review B*, 80(16):165204, October 2009.